JGR Biogeosciences

RESEARCH ARTICLE
10.1029/2022JG007085

Key Points:

- In forest ecosystems, the wood growth mainly controlled by carbon source-sink activity
- We show that wood growth and forest productivity could be connected by non-structural carbohydrates (NSC) allocation
- Constructing a direct link between annual wood growth and NSC will improve our ability to predict carbon storage and allocation in forests

Supporting Information:

Supporting Information may be found in the online version of this article.

Correspondence to:

X. Yan,
yxd@bnu.edu.cn

Citation:

Fang, J., Liu, F., Shugart, H. H., & Yan, X. (2022). Using a simple representation of non-structural carbohydrates allocation to predict wood growth in temperate forests. *Journal of Geophysical Research: Biogeosciences*, *127*, e2022JG007085. https://doi.org/10.1029/2022JG007085

Received 7 JUL 2022
Accepted 30 NOV 2022

Using a Simple Representation of Non-Structural Carbohydrates Allocation to Predict Wood Growth in Temperate Forests

Jing Fang[1,2,3], Feng Liu[1,2], Herman H. Shugart[4], and Xiaodong Yan[3]

[1]CAS Key Laboratory of Aquatic Botany and Watershed Ecology, Chinese Academy of Sciences, Wuhan, China, [2]Center of Plant Ecology, Chinese Academy of Sciences, Wuhan, China, [3]State Key Laboratory of Earth Surface Processes and Resource Ecology, Beijing Normal University, Beijing, China, [4]Department of Environmental Sciences, University of Virginia, Charlottesville, VA, USA

Abstract Wood growth is an important process of carbon sequestration and plant physiology in forest ecosystems. Hence, understanding and predicting wood growth is central to quantifying forest carbon cycling. Current dynamic global vegetation models (DGVMs) are mainly driven by carbon inputs (e.g., Gross Primary Production, GPP). However, observations indicate that wood growth is often independent of carbon flux at the annual scale. Here, we revised a DGVM, FORCCHN2 model, to use the active non-structural carbohydrates (NSC) pool and slow NSC pool (i.e., represented temporary and long-term NSC storage, respectively), and to integrate the stored NSC with annual wood growth. For the diameter increments (ΔDBH) and aboveground wood growth of 506 trees in 32 plots of Harvard Forest, we tested the NSC allocation coefficients from 5% to 95%. The predictions reproduced 31.2%–55.1% of individual-tree ΔDBH and 36.8%–43.0% of the aboveground wood increment. Trees of shade-intolerant species invested more of their available carbon resources (i.e., NSC storage) into wood growth than shade-tolerant species. Specifically, the shade-tolerant trees consumed approximately 32% NSC storage by wood growth at the annual scale, while the shade-intolerant trees consumed about 90%. Our study provides a simple framework that constructs a direct link between annual wood growth and NSC dynamics. The findings highlight the need for research into NSC storage and allocation in trees, particularly in considering NSC allocation strategies of different tree species.

Plain Language Summary Wood growth is critical to the evaluation of plant physiology and carbon sequestration in forest ecosystems. Most previous studies allocate daily photosynthesis to predict wood increment, which leads to the inconsistency between the predictions and measurements of wood growth at the annual scale. We linked daily and yearly non-structural carbohydrates (NSC) pools to wood growth performance by an NSC dynamics model. We evaluated the validity of this model using DBH increments, carbon flux (e.g., Gross Primary Production), aboveground woody growth increment, and annual NSC dynamics at Harvard Forest. In this work, we provided a framework to explore and explain the pattern of annual wood growth and carbon allocation.

1. Introduction

The carbon stored by trees through growth is critical to the evaluation of carbon sequestration in forest ecosystems (Eckes-Shephard et al., 2021; Huang et al., 2020). Substantial research on tree growth has focused on biomass variation according to tissue, for example, leaf, fine roots, and woody tissue (Schiestl-Aalto et al., 2015). Wood growth is the principal contributor to tree carbon consumption. Essentially, the carbon sequestration potential of a "tree" lies in its stocking of carbon as wood biomass. For example, the carbon sink due to wood typically represents ~20% of annual photosynthate in temperate trees (Babst et al., 2014; Delpierre et al., 2016; Wilkinson et al., 2012). Nonetheless, carbon sequestration by wood growth remains one of the least constrained parts of the current global carbon cycle evaluation and also leads to uncertainty of future CO_2 predictions (Friedlingstein et al., 2014; Quéré et al., 2018).

The growth of wood is a complex process, controlled by an ensemble of environmental and internal drivers (Delpierre et al., 2016). One approach to quantify and predict wood growth, as well as to evaluate forest carbon flux is through dynamic global vegetation models (DGVMs). These models predict the dynamic wood growth of individual tree or trees based on a "carbon source-centric" method because the carbon stored in wood comes

from photosynthesis or productivity directly (Delpierre et al., 2016; Fatichi et al., 2014, 2019; Friend et al., 2019; Merganičová et al., 2019; Xu & Trugman, 2021). However, some evidence indicates that the wood growth is decoupled with the carbon flux produced at the annual scale (Babst et al., 2014; Gea-Izquierdo et al., 2014; Richardson et al., 2013; Rocha et al., 2006). The carbon allocated to wood growth may come from the photosynthates that have been acquired in the short-term and up to several years (Gaudinski et al., 2009). Discrepancies between wood growth and carbon flux may arise from the non-structural carbohydrates (NSC) storage (Teets et al., 2018).

The NSC produced by photosynthesis is the sum of soluble sugars and starch, and it provides the substrates for vital activities (Hartmann & Trumbore, 2016). The NSC storage supports tree metabolism and growth when the immediate photosynthesis is limited by canopy phenology or stress, offering resilience in times of stress (Richardson et al., 2013). Würth et al. (2005) estimated that the total NSC pool in a tropical forest ecosystem accounts for a high percentage of forest biomass, which indicates the NSC pool is an important part of the forest carbon budget. However, the NSC pool in the DGVMs as originally designed is as a buffer between the carbon source and sink (Friend et al., 2014). Recent studies have indicated that NSC may play a more active role in estimating tree growth. For example, Schiestl-Aalto et al. (2015) used the carbon allocation sink source interaction (CASSIA) model for predicting NSC dynamics and inter-annual growth variation in Scots pine (*Pinus sylvestris*). As an adaptive strategy, the need to balance competition for resources causes a tree to invest large amounts of NSC in supporting wood growth (Dietze et al., 2014). Thus, integrating the NSC pool and the key processes of NSC allocation for wood growth at the annual scale into DGVMs is an efficient method to estimate carbon balance. However, the relationship between NSC and wood growth remains uncertain, which requires further understanding and evaluation.

Existing attempts to understand this relationship are based on hydraulics and cambium activities, which may make these models overly complex to apply in DGVMs (Eckes-Shephard et al., 2021). For example, Hölttä et al. (2010) used the pressure-flow hypothesis and sugar dynamics in 20 tree segments to predict the growth of stem diameter. On this basis, Schiestl-Aalto et al. (2015) use the CASSIA model to further increase complexity by modeling cell development in the cambium with the dynamics of NSC. These methods explain the wood growth on a micro-scale and require many parameters and input variables such as cell elasticity, cell plasticity, hydraulic conductance, water potential, turgor pressure, and sugar concentration. Much can be learned from these detailed processes or models. However, a simpler method is needed to represent the relationship between wood growth and NSC allocation in a DGVM (Eckes-Shephard et al., 2021). For example, these models need to consider several physiological parameters based on field measurements, which makes them difficult to apply in DGVMs (Fatichi et al., 2019). To simplify the modeling processes, a recent study used the different proportions of NSC to make inferences about the allocation to belowground symbionts (Schiestl-Aalto et al., 2019). In addition, DGVMs also need to consider the NSC allocation strategy found in different tree species. Poorter and Kitajima (2007) found that shade-tolerant species may allocate a larger proportion of NSC to NSC storage rather than to growth than shade-intolerant species. NSC reserves in shade-tolerant species are needed to endure low-light conditions in some cases or to recover from the non-growing season, in others.

A previous DGVM, the FORCCHN2 model, predicts the NSC dynamics at the daily scale by using a single NSC pool (Fang et al., 2020). Here, we intend to explore the relationship between NSC allocation and wood growth and quantify the carbon consumed by wood growth. To this end, we revised the FORCCHN2 model to the double NSC pools (i.e., NSC active pool and NSC slow pool) and hypothesized that part of the stored NSC in the previous years and the produced NSC in the current year were used for wood growth. The NSC active pool is used to maintain the daily vital activities of trees (Figure 1). Complementary, the NSC slow pool is considered as the NSC storage pool to keep their metabolism during carbon deficit periods (Richardson et al., 2013). The revised model allows tree growth to be decoupled from immediate Gross Primary Productivity (GPP) and Net Primary Productivity (NPP). The wood biomass balance (unit: kg C m^{-2}) and the NSC for wood growth were used to explain the variation in the radial growth. We assumed that wood growth was related to NSC and then explored the different proportions of NSC consumption (5%–95%) for wood growth of shade-tolerant and shade-intolerant species in this forest. Using data from the Harvard Forest, we tested the model-predicted performance for wood growth by using the diameter at breast height increments (ΔDBH) of individual trees.

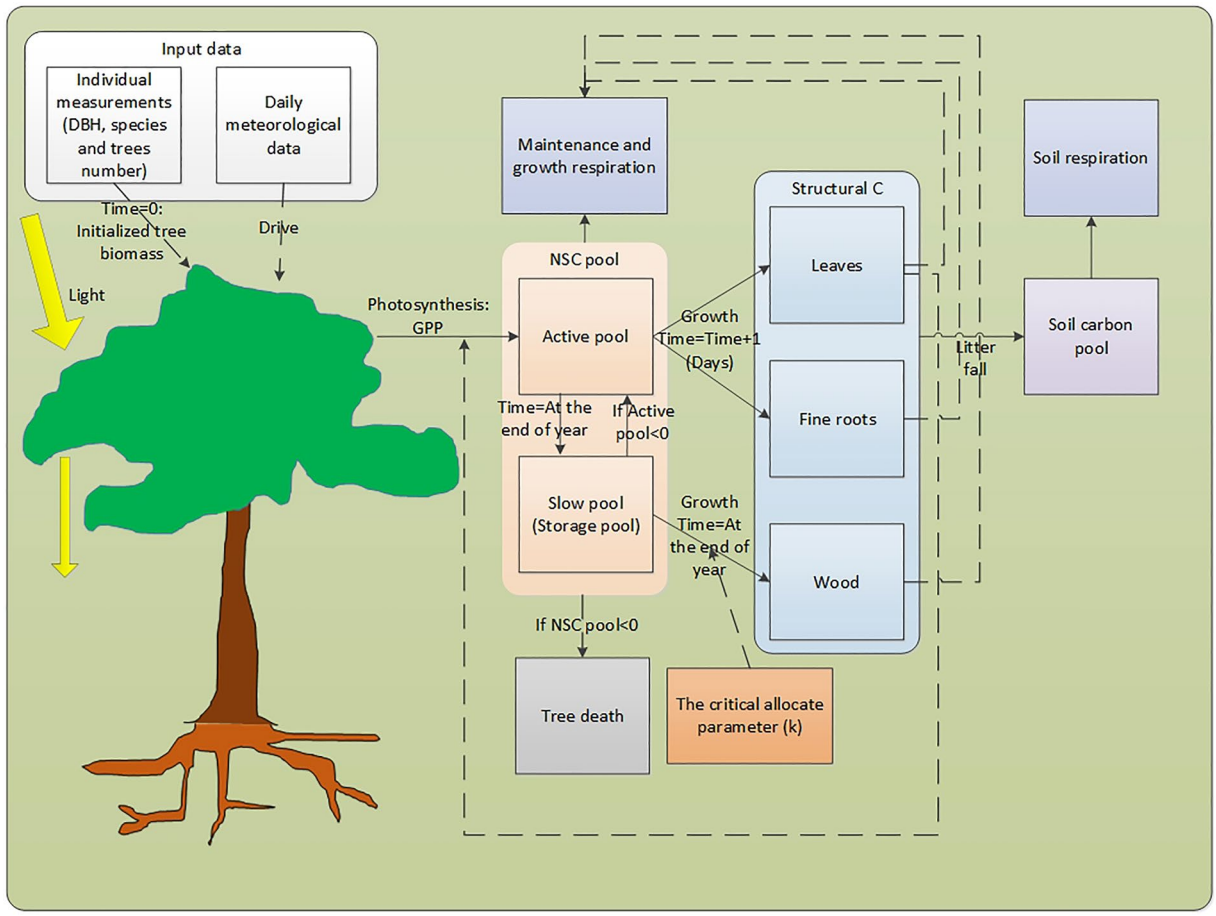

Figure 1. Schematic representation of the FORCCHN2 model. The dotted lines represent the input processes; the solid lines represent the flows of carbon. NSC: non-structural carbohydrates.

2. Materials and Methods

2.1. Study Site

The measured plots (32 plots) were located within the Harvard Forest, Massachusetts, USA (42°54′N and 72°17′W), an important part of Harvard University's Long Term Ecological Research program. These labeled plots circular plots had a 10 m radius (area: 314 m^2) and were located in the footprint of the Environment Measurement Station (EMS) tower. These labeled plots were separated by 100 m (Figure S1 in Supporting Information S1: plot map). The Harvard Forest had a mean annual temperature of 8.7°C, mean annual precipitation of 1,300 mm. The annual climate of Harvard Forest during 2000–2020 had shown in Figure S2 in Supporting Information S1. The forest type of Harvard forest was the deciduous broad-leaf forest, and the dominant tree species were red maple (*Acer rubrum*) and red oak (*Quercus rubra*).

2.2. Inventory Data

The inventory data was taken from the Harvard Forest Data Archive: HF069 (W. Munger & S. Wofsy, 2020a). The DBH of each tree with a DBH greater than 10 cm was measured by an attached dendrometer's expansion (or contraction) to the nearest millimeter. The DBH data were taken with digital calipers. To match the observed time of carbon flux, we chose the measured inventory time from 2000 to 2020. In this data set, the trees were remeasured annually, but a lot of trees were not observed continuously and missed the corresponding records. To keep as many trees as possible and test the long-time predicted performance, we chose the DBH data with a time interval of 5 years (i.e., the period of ΔDBH was 2000–2005, 2000–2010, 2000–2015, and 2000–2020). There were 506 live trees with 2024 ΔDBH data in the 32 plots (i.e., each tree has 4 ΔDBH data). The detailed

information of each plot includes the number of trees, DBH range, and main tree species (Table 1). According to the database of United States department of agriculture Forest Service Southern Research Station, we divided all trees into deciduous broadleaf with shade tolerance or intolerance and evergreen needleleaf with shade tolerance or intolerance (Table S1 in Supporting Information S1: the detailed information of each tree species).

For testing the yearly dynamics of wood, we calculated the aboveground wood increment (AGWI) during 2000–2020. The AGWI was defined as the difference in a current year's aboveground wood biomass (AGWB) and the previous year's AGWB (i.e., in consecutive years):

$$AGWI_{k,j} = AGWB(DBH)_{k,j+1} - AGWB(DBH)_{k,j} \quad (1)$$

Where k meant the kth tree; j meant the jth year; $j + 1$ meant the next year of the jth year. In each year, the AGWI was calculated by the trees with the valid DBH records and we did not calculate the AGWI of the trees that missing the record in this year. In 2020, the AGWI equaled the AGWB of October minus the AGWB of April. The AGWB was calculated by DBH and species-specific allometric equations (i.e., extracted from the HF069-17). All allometric equations had shown in Table S1 in Supporting Information S1.

2.3. Carbon Flux and Climate Data

The carbon flux data observed by the Eddy Covariance instrument of EMS towers, and the used data sources were mainly coming from two parts: one was obtained from the archived FLUXNET2015 data set (The available period of carbon flux was 2000–2012) (Pastorello et al., 2020); another was from the HF004 of Harvard Forest Data Archive (The available period was 2013–2019) (W. Munger & S. Wofsy, 2020b). Note that the Net Ecosystem Productivity (NEP) value was equal to the negative value of the Net Ecosystem CO_2 Exchange (NEE, from the data set directly). The GPP value was equal to the NEP plus Ecosystem Respiration (ER, from the data set directly). The NPP data was equal to the NEP plus Soil Respiration (SR), which was extracted from Finzi et al. (2020) (the available period was 2000–2015). Therefore, the available period of GPP and NEP was 2000–2019 and the available period of NPP was 2000–2015.

We used the daily climate data to drive the model. These data included the daily maximum and minimum air temperature (°C), precipitation (mm), relative humidity (%), wind speed (m s^{-1}), atmospheric pressure (hPa), total solar radiation (W m^{-2}), and CO_2 concentration (ppm). The climate data was sourced from the FLUXNET2015 data set (available period: 2000–2012) and HF001 of Harvard Forest Data Archive (available period: 2013–2020) (Boose, 2022). The corresponding CO_2 concentration was from the FLUXNET2015 data set (available period: 2000–2012) and HF0197 of Harvard Forest Data Archive (available period: 2013–2020) (W. Munger & J. Hadley, 2022).

2.4. Model Description

The individual-based carbon model, FORCCHN2 (Fang et al., 2020), is driven by daily climate data and predicts annual growth with the carbon dynamics for each tree. The model predicts the carbon budget by coupling soil carbon cycle models on a plot scale. Depending on the process considered, FORCCHN2 runs on daily and annual timesteps (Figure 1). For an individual tree, the principal daily processes are photosynthesis, maintenance respiration, carbon allocation, and soil respiration. This model calculates the carbon allocation of the individual tree from the NSC production, demand, and storage. In this study, we divided the single NSC pool of the original FORCCHN2 into two pools (i.e., the NSC active pool and the NSC slow pool). NSC active pool represented the daily carbon dynamics of photosynthetic productivity, maintenance respiration, growth respiration, and growth carbon demand. NSC slow pool represented the annual NSC storage pool. These NSC pools allowed the growth of different parts of the tree to be decoupled from instantaneous carbon flux. For example, the slow pool provided the necessary carbon for the requirements of the individual tree when contemporaneous photosynthetic production (i.e., GPP, a type of carbon flux) and the NSC fast pool were insufficient to maintain growth or respiration. Meanwhile, we revised the allocated parameters of the NSC storage pool at the yearly step to explore the proportion of carbon consumption by wood growth.

Table 1
The Detailed Information of Each Plot

Plot's no.	Trees' number	DBH range in 2000 (cm)	Main tree species	Total
A1	12	13.67–56.48	*Betula alleghaniensis*, *Acer rubrum*	
B1	12	13.25–48.2	*Acer rubrum*, *Quercus rubra*	
C1	14	11.55–56.87	*Quercus rubra*, *Tsuga canadensis*	
D1	16	10.55–47.09	*Acer rubrum*, *Quercus rubra*, *Quercus velutina*, *Pinus strobus*	
E1	10	10.53–47.01	*Betula alleghaniensis*, *Acer rubrum*, *Tsuga canadensis*	
F1	16	10.38–56.81	*Acer rubrum*, *Pinus resinosa*	
G1	17	10.12–45.02	*Pinus resinosa*	
H1	18	13.37–48.29	*Acer rubrum*, *Pinus strobus*, *Quercus rubra*	
A2	10	11.92–41.55	*Acer rubrum*, *Quercus velutina*	506 trees, including 193 shade-tolerant trees and 313 shade-intolerant trees.
B2	8	12.38–62.32	*Acer rubrum*, *Betula alleghaniensis*	
C2	12	10.84–53.89	*Acer rubrum*, *Quercus rubra*	
D2	9	10.43–39.61	*Acer rubrum*	
E2	21	13.12–38.53	*Acer rubrum*, *Quercus rubra*, *Pinus resinosa*	
F2	17	10.01–57.08	*Acer rubrum*, *Betula lenta*	
G2	20	12.37–48.59	*Tsuga canadensis*	
H2	24	11.64–59.43	*Tsuga canadensis*, *Acer rubrum*, *Quercus rubra*	
A3	12	11.35–55.36	*Acer rubrum*, *Quercus rubra*	
B3	19	13.04–43.91	*Acer rubrum*, *Quercus rubra*	
C3	19	13.17–39.31	*Acer rubrum*, *Betula alleghaniensis*	
D3	11	12.85–59.21	*Acer rubrum*, *Quercus rubra*	
E3	17	10.28–52.03	*Acer rubrum*, *Quercus rubra*	
F3	13	11.12–56.91	*Tsuga canadensis*, *Betula alleghaniensis*, *Pinus strobus*	
B4	18	10.39–34.13	*Acer rubrum*, *Betula populifolia*	
C4	22	10.78–40.29	*Acer rubrum*, *Quercus rubra*, *Fraxinus americana*	
D4	12	10.25–45.39	*Acer rubrum*, *Prunus serotina*	
E4	29	11.22–42.32	*Acer rubrum*, *Fraxinus americana*, *Pinus strobus*	
F4	22	12.8–66.39	*Quercus rubra*, *Acer rubrum*, *Fraxinus americana*	
G4	6	17.4–32.89	*Acer rubrum*, *Betula alleghaniensis*	
C5	12	10.31–31.38	*Acer rubrum*, *Quercus rubra*	
D5	9	10.82–33.85	*Acer rubrum*	
E5	27	11.22–50.12	*Tsuga canadensis*, *Pinus strobus*, *Acer rubrum*	
F5	22	10.83–38.99	*Acer rubrum*, *Quercus rubra*, *Pinus strobus*	

Daily step For each individual tree, the photosynthesis (GPP), maintenance respiration (R), growth respiration (R^G), and carbon use to growth (G) were assumed to determine the daily changes of the NSC active pool (NSC_{active}) (Fang et al., 2020):

$$\frac{dNSC_{active}}{dt} = GPP(t) - \sum R_m(t) - \sum R_i^G(t) - \sum G_i(t) \quad (2)$$

Where t is the day of the year; the subscript m denotes the biomass fraction for leaves, wood, and fine roots; the subscript i denotes the biomass fraction for leaves and fine roots, respectively. The GPP, R^G, and R were calculated by the original FORCCHN2 model (Method S1 in Supporting Information S1). The G of leaves and fine roots were also calculated by Method S1 in Supporting Information S1.

Yearly step To maintain sufficient efficiency and simple representation, the model assumed that NSC was allocated to the growth of leaves and fine roots during the daily processes, and the NSC allocation for the growth of wood during the yearly processes. Thus, the model used the NSC storage pool (i.e., NSC slow pool: NSC_{slow}) in a given year to support the annual wood growth (G_{wood}) (Figure 1). The NSC allocation for wood growth was determined by a critical allocation parameter (k):

$$NSC_{slow}(j_{end}) = NSC_{slow}(j_0) + NSC_{active}(j_{end}) \quad (3)$$

$$NSC_{slow}((j+1)_0) = NSC_{slow}(j_{end}) - G_{wood}(j) \quad (4)$$

$$G_{wood}(j) = k \cdot NSC_{slow}(j_{end}) \quad (5)$$

Where j meant the jth year; $j+1$ meant the next year of the jth year; j_{end} meant the end day at jth year; j_0 meant the first day at jth year; $(j+1)0$ meant the first day at $j+1$th year. Note that the value range of k was 0–1.

The wood biomass of a given year was calculated by the wood biomass of the previous year and wood growth:

$$B_{wood}(j) = B_{wood}(j-1) + G_{wood}(j) \quad (6)$$

$$B_{wood}(j) = f_{wood}(D + dD, H + dH, b + db, hr, astem) \quad (7)$$

$$B_{wood}(j-1) = f_{wood}(D, H, b, hr, astem) \quad (8)$$

$$dH = cp \cdot dD \quad (9)$$

Where j meant the jth year; $j-1$ meant the previous year; D was the tree's DBH; dD was the DBH increment in 1 year; H was the tree height; dH was the height increment in 1 year; b was the height of twig; db was the height of twig increment in 1 year; hr was the depth of root; $astem$ was the volume weight of wood; cp was a constant, which depended on the light gradient (Table S2 in Supporting Information S1). Note that we used the "binary search algorithm" to calculate the optimal dD (the initialized range of dD was set to 0–20 cm), which made the left part equal to the right part in Equation 7. The f_{wood} was calculated by the allometric equations (Method S2 in Supporting Information S1), and the simulated performance of this method had shown in Figure S3 in Supporting Information S1.

2.5. Model Initialization

The assumptions from the original FORCCHN2 model were used to initialize and calculate the vegetation information by using the DBH of the individual trees (Method S2 in Supporting Information S1). The initial NSC active pool in each year was assumed as 0 on the first day of the year. For the initial NSC storage pool (slow pool) in Harvard Forest, Furze et al. (2019), Fang et al. (2020), and Barker Plotkin et al. (2021) measured and concluded that the NSCs relative to wood biomass was 2%–5%. We compared the ΔDBH results from the different initial NSC% (set as 2%–5% with a 1% interval), and we assumed the NSC% to be 3% of wood biomass in this work (Figure S4 in Supporting Information S1). Depending on the tree species, the plant functional types (PFTs) of all plots in the present work were for deciduous broadleaf trees and evergreen needle leaf trees. Every type had its respective physiological and ecological parameters (Table S2 in Supporting Information S1). To compute the light competition among the different trees, we used a standard gap-model formulation to describe the vertical radiation environment (Equation S29 in Supporting Information S1). To explore the proportion of NSC allocation

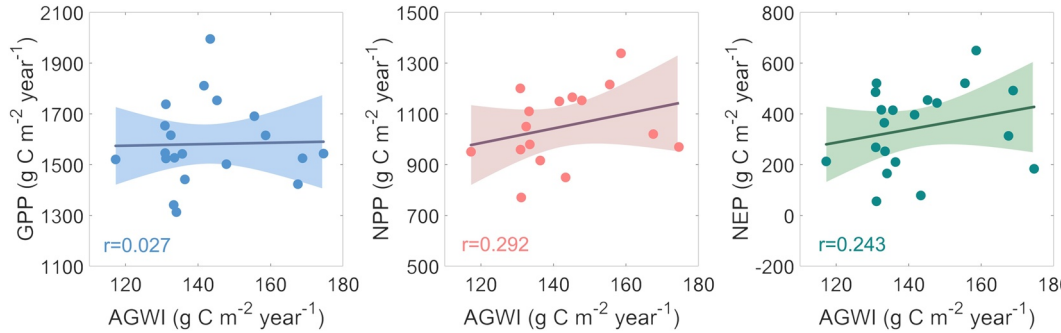

Figure 2. Correlation of annual aboveground wood growth increment (aboveground wood increment) with carbon flux at the 32 plots of Harvard Forest. The carbon fluxes include (a) the gross primary productivity (GPP), the available period is 2000–2019, (b) Net Primary Productivity, the available period is 2000–2015, and (c) Net Ecosystem Productivity, the available period is 2000–2019.

by wood growth, we set the annual allocation parameter (k) from 0.05 to 0.95 with a 0.05 interval (Equation 5). For calculating the k value more accurately, we then set an 0.01 interval between the two 0.05 intervals with the best model performance, Other processes and parameters of this model had shown in Method S1 and S2, Table S2, Table S3, and Table S4 in Supporting Information S1.

2.6. Statistical Analyses

The predicted results were evaluated against measured observations, which included the daily GPP, daily NEP, ΔDBH, and AGWI. We used Pearson correlation coefficient (r), correlation coefficient square (r^2), model efficiency (E), root mean square error ($RMSE$), and bias ($bias$):

$$E = 1 - \frac{\sum_{i=1}^{n} (X_i - Y_i)^2}{\sum_{i=1}^{n} \left(Y_i - \overline{Y}\right)^2} \tag{10}$$

$$\text{bias} = \frac{1}{n} \sum_{i=1}^{n} (X_i - Y_i) \tag{11}$$

Where the X_i and Y_i are the predicted and measured data, respectively; $\overline{X}$ and $\overline{Y}$ represent their mean values. The range of E was $-\infty$ to 1, and E close to 1 means a perfect match between the predictions and measurement.

3. Results

3.1. Correlation of AGWI and Carbon Flux

During 2000–2020, the observed carbon fluxes were compared to the measured AGWI in the Harvard Forest. The annual carbon fluxes, including GPP, NPP (calculated by Equation S48 in Supporting Information S1), and NEP (calculated by Equation S49 in Supporting Information S1) showed no correlation with annual AGWI (Figure 2: r = 0.027, 0.292, 0.243 of GPP, NPP, and NEP), indicating that the wood growth was not determined by the amount of carbon fluxes at the annual scale.

3.2. The Proportion of Carbon Consumption by Wood Growth

Here, we used the DBH increment in a given period (ΔDBH) to evaluate the predicted performance of wood growth. Trees were divided into shade-tolerant and shade-intolerant species. The measured ΔDBH was compared to the 22 predictions (i.e., the results of 22 different k values) in the 32 plots. Each plot produced a statistical outcome (i.e., predicted vs. measured ΔDBH of every tree in the given plot), and the results of all plots were drawn as the box plot.

For the predicted wood growth for different annual carbon allocated proportion (k, see Figures 3 and 4, and Figure S5 in Supporting Information S1), all results (i.e., predicted *vs*. measured) of shade-tolerant trees had similar and

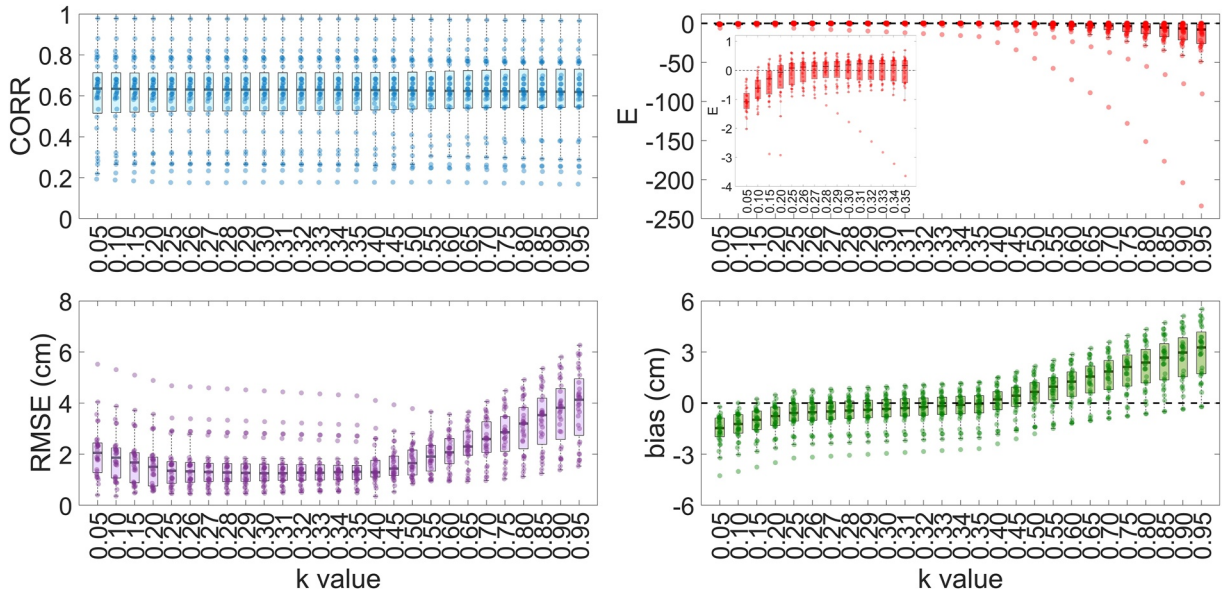

Figure 3. The statistical results of measured versus predicted ΔDBH of the shade-tolerant trees in the 32 plots of Harvard Forest. Each box has 32 data and each point represents 1 data. These results are based on 27 different values of the annually allocate parameter (*k*). The results include four time periods of ΔDBH: 2000–2005, 2000–2010, 2000–2015, and 2000–2020. CORR: correlation coefficient (i.e., *r*); E: model efficiency; RMSE: root mean square error.

significant correlations (the range of *r* median was between 0.63 and 0.64, and the significance *p* was less than 0.05). The best predicted performance occurred in the range of $k = 0.25$–0.35. When $k = 0.32$, one saw the highest model efficiency (the *E* median of $k = 0.32$ was larger than other values) (Figure 3). With $k = 0.30$, the model yielded the best performance of *RMSE* (the *RMSE* median was 1.25 cm) and $k = 0.35$ produced the minimum *bias* (the *bias* median was −0.04 cm). Values of $k = 0.95$ had the poorest performance with respect to all statistical results. Overall, these results indicated that shade-tolerant trees consumed 32% amount of the annual NSC storage pool had a better performance to support the wood growth than other *k* values.

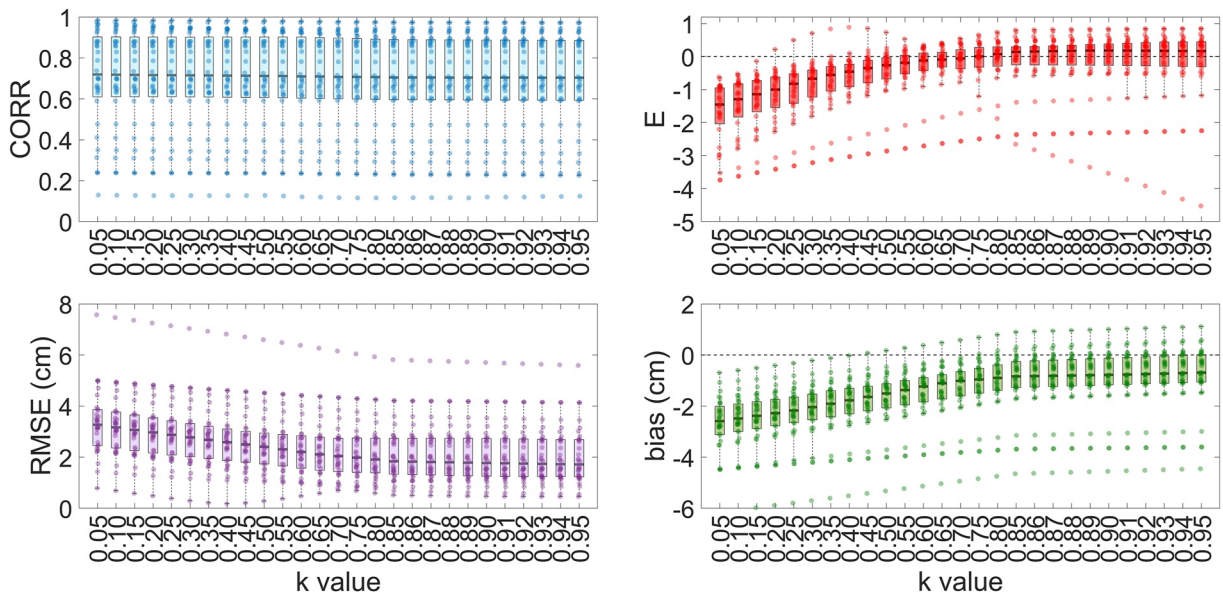

Figure 4. The statistical results of measured versus predicted ΔDBH of the shade-intolerant trees in the 32 plots of Harvard Forest. These results are based on 27 different values of the critical allocate parameter (*k*). The results include four time periods of ΔDBH: 2000–2005, 2000–2010, 2000–2015, and 2000–2020. CORR: correlation coefficient (i.e., *r*); E: model efficiency; RMSE: root mean square error.

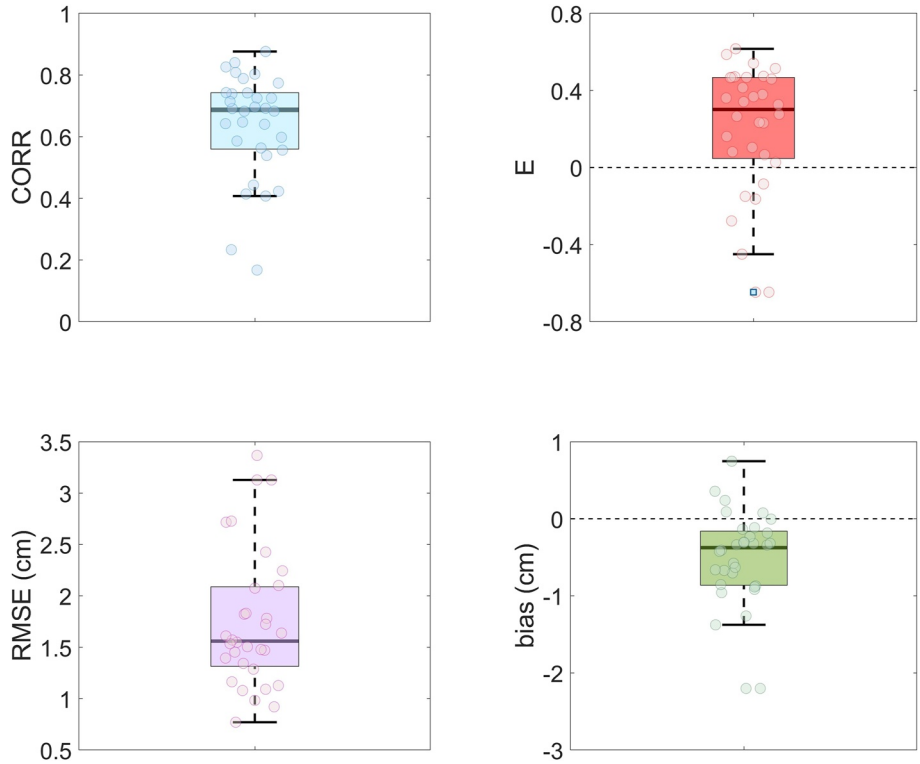

Figure 5. The statistical results of measured versus predicted ΔDBH of all trees in the 32 plots of Harvard Forest. These results are based on the value of k_{ST} equal to 0.32 (ST: shade-tolerant) and the value of k_{SIT} equal to 0.90 (SIT: shade-intolerant). The results include four time periods of ΔDBH: 2000–2005, 2000–2010, 2000–2015, and 2000–2010. CORR: correlation coefficient (i.e., *r*); E: model efficiency; RMSE: root mean square error.

The results of shade-intolerant trees presented obvious differences from the shade-tolerant trees (Figure 4). The range of r median of all k values was around 0.70. Although all predicted results were positively correlated with measurements, the result of $k = 0.90$ had a higher median of model efficiency than other values of k. The median of model efficiency was 0.19, *RMSE* was 1.77 cm, and the model underestimated 0.78 cm ΔDBH when the allocated proportion $k = 0.90$. These results indicated that 90% of the annual NSC storage pool used by shade-intolerant trees showed better performance to support the wood growth than other k values.

Both the allocated proportion $k = 0.32$ of shade-tolerant trees and the allocated proportion $k = 0.90$ of shade-intolerant trees were applied in the model (Figure 5 and Figure S6 in Supporting Information S1). The FORCCHN2 model captured the 31.2%–55.1% variance (i.e., interquartile range of r^2, the correlation coefficient (r) square) of ΔDBH, and the model efficiency ranged from −0.02 to 0.46 (Figure 5). The predictions underestimated 0.20–0.88 cm of measurements, and the *RMSE* of the compared result was 1.36–2.09 cm. These results indicated that the parameters and the model could reproduce the dynamics of wood growth in these plots. In addition, we evaluated the mean predicted and measured ΔDBH of the different tree sizes (Figure S7 in Supporting Information S1). We divided the all trees into four sizes by classified DBH (i.e., the total number of trees was 506; the 10–16.5 cm DBH had 126 trees, the 16.5–23.4 cm DBH had 128 trees, the 23.4–33.0 cm DBH had 126 trees, the DBH larger than 33.0 cm had 126 trees). The model underestimated ΔDBH for all tree sizes and the value of underestimation increased with the sizes.

3.3. AGWI and NSC Dynamics

We used the aboveground wood growth increment (AGWI) to test the overall predicted performance of wood growth in Harvard Forest (Figures 6 and 7a). The range of the best model efficiency of shade-tolerant trees and shade-intolerant trees had occurred when k equaled 0.25–0.35 and 0.85–0.95, respectively. Similarly, we found that $k = 0.32$ of shade-tolerant trees and $k = 0.90$ of shade-intolerant trees were more suitable for predicting

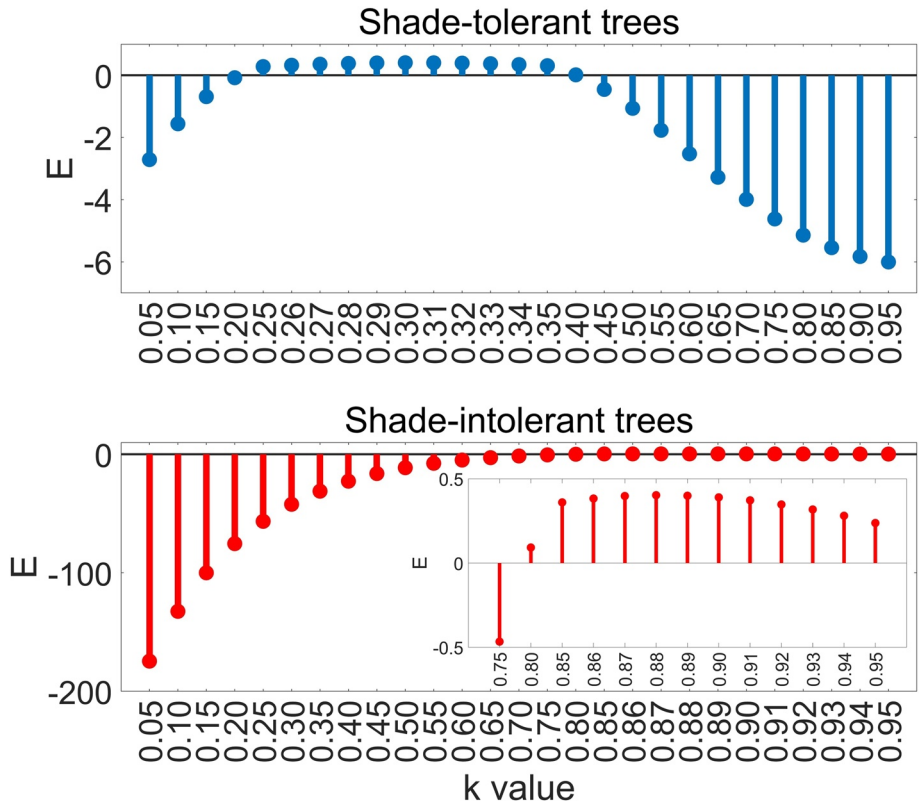

Figure 6. The model efficiency (E) of measured versus predicted aboveground wood increment of the shade-tolerant trees and shade-intolerant trees in all plots of Harvard Forest. These results are based on 27 different values of the critical allocate parameter (k).

AGWI than other k values. In general, the trends and magnitudes of the best predictions were generally consistent with measured data (Table 2: $r = 0.65$ and $E = 0.39$). However, differences existed between the simulations and measurements, such as the model overestimated AGWI in some years and underestimated AGWI in other years. The variation of NSC consumption by wood growth was similar to the variation of predicted AGWI, as well as

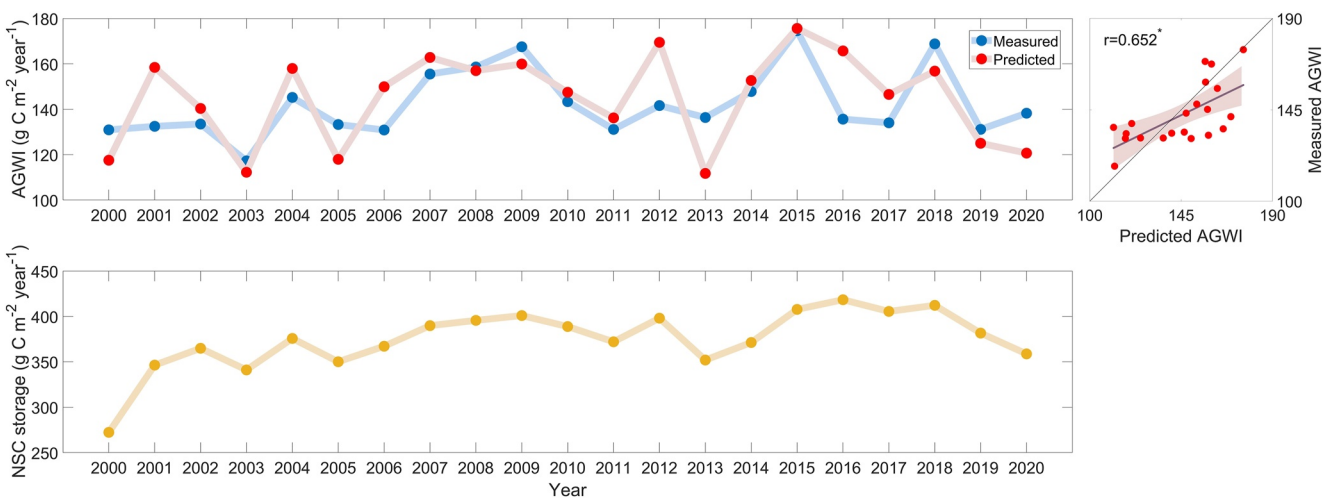

Figure 7. (a) Is measured versus predicted AWGI in Harvard Forest during 2000–2020, and the right is the corresponding scatter plot; (b) is the predicted non-structural carbohydrates storage increment at the annual scale. These results are based on the value of k_{ST} equal to 0.32 (ST: shade-tolerant) and the value of k_{SIT} equal to 0.90 (SIT: shade-intolerant). AGWI: aboveground wood growth increment; NSC: non-structural carbohydrates. * means the significance is less than 0.05.

Table 2
Comparison of Measured and Predicted Results

	Statistical value			
	r	E	RMSE	Bias
GPP	0.923	0.839	1.986 (g C m^{-2} d^{-1})	−0.566 (g C m^{-2} d^{-1})
NEP	0.862	0.670	2.078 (g C m^{-2} d^{-1})	0.554 (g C m^{-2} d^{-1})
AGWI	0.652	0.390	15.118 (g C m^{-2} $year^{-1}$)	2.579 (g C m^{-2} $year^{-1}$)
ΔDBH (median)	0.687	0.301	1.559 (cm)	−0.375 (cm)

Note. The Results of ΔDBH are From the First Quartile to the Third Quartile in All Plots. *r*: Correlation Coefficient; E: Model Efficiency; RMSE: Root Mean Square Error; GPP: Gross Primary Productivity; NEP: Net Ecosystem Productivity; AGWI: Aboveground Wood Growth Increment.

the NSC storage increment (Figure 7b). This was in accord with our assumption that a portion of the NSC storage pool in the current year was allocated to the NSC storage increment (Equations 3–5 and Figure 1).

4. Discussion

4.1. Model Performance of Wood Growth

Numerous previous studies used the allocation strategies of wood growth based on carbon flux pools, but increasing evidence explains that wood formation relies on a combination of current and previously stored NSC (Teets et al., 2018). To illustrate the link between NSC pools and wood growth, we revised an individual tree-based carbon model (FORCCHN2) to integrate the annual wood growth with carbon allocation through the NSC pools. The model simultaneously evaluated forest individual tree DBH increments (ΔDBH) and carbon flux in the Harvard Forest. This work suggested considering using NSC active and storage pool simultaneously in the DGVMs to predict tree growth dynamics.

The annual AGWI is not significantly correlated with the annual carbon flux in *situ* (Figure 2). These results are consistent with the observations in other forests and suggest that the wood growth does not often depend on annual GPP or NEP (Babst et al., 2014; Mund et al., 2010). Although wood is carbon storage in trees, its annual growth should be distinguished from other parts of the tree because it is perennial (Delpierre et al., 2016). The predicted AGWI explained 42.5% (i.e., r^2, the correlation coefficient r square) interannual variations of the measured AGWI, which indicates that estimates of AGWI at the yearly scale can be obtained by the reasonable allocation of the NSC pool (Figure 7). The NSC allocation for wood growth is difficult to measure directly, and we use the revised FORCCHN2 model to describe this allocation at the annual scale. The overall performance of the tree ΔDBH predictions in the 32 plots presents that the method of NSC allocation to simulate tree growth is feasible. Although wood growth was modeled using the approach of NSC allocation, the annual DBH increment was treated in a relatively simple manner, with the objective of providing a framework for carbon consumption related to wood biomass.

Usually, the trees do not use all NSC for wood growth because the growth is controlled by current environmental conditions or endogenous mechanisms (Mund et al., 2010). According to this hypothesis, a part of the stored and produced NSC in the current year is consumed by wood growth, while the remaining portion of the NSC entered the storage pool. Then, the annual DBH increment is calculated by wood biomass of adjacent years. This method is considered reasonable because a "tree" could use a lot of NSC for structural growth, which makes itself competitive for external resources (Guillemot et al., 2017). The annual NSC storage pool is not only as a buffer pool for photosynthesis and carbon consumption, and this pool also provides the necessary carbon source for trees when faced with unpredictable stressors (e.g., drought) (Furze et al., 2019). Although there are some disparities between the predicted and measured ΔDBH, given the wide variety of wood formations, the reasonable success of a growth model as simple as ours is unexpected. The model merits further development focusing on the mechanisms responsible for the processes of wood growth. For example, the water in the soil could limit the wood growth, but our model assumed that the wood growth was only indirectly influenced by the soil water. Some evidence suggests that water stress has an effect on the DBH increment through the activity of cambial cells (Guillemot et al., 2017). Eckes-Shephard et al., 2021 directly used the soil water in modeling wood increment

in DGVMs. Besides, wood phenology has been identified to control the interannual variability of wood growth (Delpierre et al., 2016).

4.2. Allocation of NSC in Different Tree Species

Multiple factors can influence the NSC allocation, including the environmental effects (e.g., the climate conditions and soil water content) and tree physiology (e.g., PFT). Among these factors, the species of the tree itself is an important factor (Babst et al., 2014). Our results present that shade-intolerant trees spend more available carbon resources to support wood growth than shade-tolerant trees (90% vs. 32%). Under the conditions set by the model, the two trees of similar size showed the shade-intolerant species produced 1.99 kg C (i.e., GPP) with photosynthesis, consumed 0.42 kg C (21% of GPP) for structural growth of leaf and fine roots, and released 1.11 kg C (56% of GPP) as maintenance and growth respiration during the year (Figure S8 in Supporting Information S1). Correspondingly, the shade-tolerant species produced 6.18 kg C with photosynthesis, consumed 0.62 kg C (10% of GPP) for structural growth of leaf and fine roots, and released 1.72 kg C (28% of GPP) as maintenance and growth respiration (Figure S8 in Supporting Information S1). The results indicated that the difference of NSC allocation between the two species mainly comes from photosynthesis. The photosynthesis is controlled by leaf area (Equation S2 in Supporting Information S1) and this area is determined by the coefficient of leaf area ($cLAI_L$ in Equation S47 and Table S2 in Supporting Information S1, Ma et al., 2017). Besides, every species has its respective strategies for resource allocation because of the growth patterns and inter-tree competition (Pothier, 2017). In natural environments, shade-intolerant trees consume more carbon for the wood growth to compete for more light in the vertical structure, while shade-tolerant trees store more carbon to grow more leaves in the next year, which can improve light capture ability and productivity under low light conditions (Portsmuth & Niinemets, 2007). The shade-tolerant species have lower physiological plasticity than the intolerant species. Greater physiological plasticity allows shade-intolerant species to achieve rapid wood growth rates and thereby rapidly colonize early successional habitats (Walters & Reich, 1999). In a carbon allocation study from the Abitibi-Témiscamingue region of Northwestern Quebec (Goudiaby et al., 2022), the carbon allocation of a shade-tolerant species—black spruce (*Picea mariana*) to tree stem is estimated ∼35%, and a shade-intolerant species—jack pine (*Pinus banksiana*) allocated 60% carbon for tree stem. However, these results of species effect are only a preliminary exploration, and each tree species has its growth rate and NSC allocation coefficient (Brienen et al., 2006). For example, we found the model can predict the wood growth of the red maple (*Acer rubrum*) better than the black cherry (*Prunus serotina*) (Figure S9 in Supporting Information S1). The plot has the black cherry trees (D4 plot: $r = 0.168$ and $E > 0$, 4 red maple trees, 4 black cherry trees, 3 white ash trees, and 1 black oak tree) shows a lower correlation than the plot without black cherry trees (A1 plot: $r = 0.739$ and $E < 0$, 6 red maple trees, 4 yellow birch trees, and 2 red oak trees).

4.3. Uncertainties in Predicting Carbon Flux

According to the validation results, the revised model is able to reproduce the NEP of the forest (Figure S10 in Supporting Information S1 and Table 2). There are still some errors in the NEP prediction and the previous studies have summarized this phenomenon as the GPP underestimation (Moffat et al., 2007; Raczka et al., 2013). Through Equation 2, the uncertainties of carbon flux could influence the predicted performance of NSC. One reason for this underestimation is the vegetation parameters in the DGVMs are constants (Table S2 in Supporting Information S1), but the ecological characteristics of individual trees change with the surrounding environment (Reich et al., 2006; Wright et al., 2004). For example, the optimal temperature of photosynthesis in the model is constant, but the actual optimal temperature may be higher than the optimal temperature of the model (e.g., *Topt* in Table S2 in Supporting Information S1), which leads to the underestimation of GPP (Equations S1 and S5 in Supporting Information S1). Huang et al. (2019) present the optimal temperature of photosynthesis had a spatial and time variation instead of the constant.

5. Conclusion

In this study, we focus on the framework of NSC allocation by wood growth at the annual scale. Because the carbon flux shows no correlation with annual wood increments, this framework helps the DGVMs to use the NSC pools instead of carbon flux pools to predict wood growth. We also found that shade-tolerant trees invest 32% of

NSC and shade-intolerant trees invest 90% of NSC to support the wood growth in the temperate forest. Our results explore the carbon balance between growth and NSC storage, in order to gain a comprehensive understanding of the tree dynamics and the defense strategy. These findings have the potential to reduce uncertainties in predicting the future dynamics of forest vegetation and the carbon cycle.

Data Availability Statement

The inventory and allometric equations are available from the Harvard Forest Data Archive: HF069 (https://harvardforest1.fas.harvard.edu/exist/apps/datasets/showData.html?id=HF069). The carbon fluxes and climate data are extracted from the FLUXNET2015 data set (https://fluxnet.org/data/fluxnet2015-dataset/), HF004 (https://harvardforest1.fas.harvard.edu/exist/apps/datasets/showData.html?id=HF004), and HF001 (https://harvardforest1.fas.harvard.edu/exist/apps/datasets/showData.html?id=HF001). The CO_2 concentration is extracted from the HF197 (https://harvardforest1.fas.harvard.edu/exist/apps/datasets/showData.html?id=HF197).

Acknowledgments
This study was supported by the National Natural Science Foundation of China (32101349) and by a grant from the University of Virginia Center for Global Inquiry and Innovation. This study also was supported by the National Natural Science Foundation of China (31700462, 31870465) and the National Key Research and Development Program of China (Grant 2018YFC1509003).

References

Babst, F., Bouriaud, O., Papale, D., Gielen, B., Janssens, I. A., Nikinmaa, E., et al. (2014). Above-ground woody carbon sequestration measured from tree rings is coherent with net ecosystem productivity at five eddy-covariance sites. *New Phytologist*, *201*(4), 1289–1303. https://doi.org/10.1111/nph.12589

Barker Plotkin, A., Blumstein, M., Laflower, D., Pasquarella, V. J., Chandler, J. L., Elkinton, J. S., & Thompson, J. R. (2021). Defoliated trees die below a critical threshold of stored carbon. *Functional Ecology*, *35*(10), 2156–2167. https://doi.org/10.1111/1365-2435.13891

Boose, E. (2022). Fisher meteorological station at Harvard forest since 2001. In *Harvard forest data archive: HF001* (Vol. *27*).

Brienen, R. J., Zuidema, P. A., & During, H. J. (2006). Autocorrelated growth of tropical forest trees: Unraveling patterns and quantifying consequences. *Forest Ecology and Management*, *237*(1–3), 179–190. https://doi.org/10.1016/j.foreco.2006.09.042

Delpierre, N., Berveiller, D., Granda, E., & Dufrêne, E. (2016). Wood phenology, not carbon input, controls the interannual variability of wood growth in a temperate oak forest. *New Phytologist*, *210*(2), 459–470. https://doi.org/10.1111/nph.13771

Dietze, M. C., Sala, A., Carbone, M. S., Czimczik, C. I., Mantooth, J. A., Richardson, A. D., & Vargas, R. (2014). Nonstructural carbon in woody plants. *Annual Review of Plant Biology*, *65*(1), 667–687. https://doi.org/10.1146/annurev-arplant-050213-040054

Eckes-Shephard, A. H., Tiavlovsky, E., Chen, Y., Fonti, P., & Friend, A. D. (2021). Direct response of tree growth to soil water and its implications for terrestrial carbon cycle modelling. *Global Change Biology*, *27*(1), 121–135. https://doi.org/10.1111/gcb.15397

Fang, J., Lutz, J. A., Shugart, H. H., & Yan, X. (2020). A physiological model for predicting dynamics of tree stem-wood non-structural carbohydrates. *Journal of Ecology*, *108*(2), 702–718. https://doi.org/10.1111/1365-2745.13274

Fatichi, S., Leuzinger, S., & Körner, C. (2014). Moving beyond photosynthesis: From carbon source to sink-driven vegetation modeling. *New Phytologist*, *201*(4), 1086–1095. https://doi.org/10.1111/nph.12614

Fatichi, S., Pappas, C., Zscheischler, J., & Leuzinger, S. (2019). Modelling carbon sources and sinks in terrestrial vegetation. *New Phytologist*, *221*(2), 652–668. https://doi.org/10.1111/nph.15451

Finzi, A. C., Giasson, M. A., Barker Plotkin, A. A., Aber, J. D., Boose, E. R., Davidson, E. A., et al. (2020). Carbon budget of the Harvard forest long-term ecological research site: Pattern, process, and response to global change. *Ecological Monographs*, *90*(4), e01423. https://doi.org/10.1002/ecm.1423

Friedlingstein, P., Meinshausen, M., Arora, V. K., Jones, C. D., Anav, A., Liddicoat, S. K., & Knutti, R. (2014). Uncertainties in CMIP5 climate projections due to carbon cycle feedbacks. *Journal of Climate*, *27*(2), 511–526. https://doi.org/10.1175/jcli-d-12-00579.1

Friend, A. D., Eckes-Shephard, A. H., Fonti, P., Rademacher, T. T., Rathgeber, C. B., Richardson, A. D., & Turton, R. H. (2019). On the need to consider wood formation processes in global vegetation models and a suggested approach. *Annals of Forest Science*, *76*(2), 1–13. https://doi.org/10.1007/s13595-019-0819-x

Friend, A. D., Lucht, W., Rademacher, T. T., Keribin, R., Betts, R., Cadule, P., et al. (2014). Carbon residence time dominates uncertainty in terrestrial vegetation responses to future climate and atmospheric CO_2. *Proceedings of the National Academy of Sciences of the United States of America*, *111*(9), 3280–3285. https://doi.org/10.1073/pnas.1222477110

Furze, M. E., Huggett, B. A., Aubrecht, D. M., Stolz, C. D., Carbone, M. S., & Richardson, A. D. (2019). Whole-tree nonstructural carbohydrate storage and seasonal dynamics in five temperate species. *New Phytologist*, *221*(3), 1466–1477. https://doi.org/10.1111/nph.15462

Gaudinski, J. B., Torn, M. S., Riley, W., Swanston, C., Trumbore, S. E., Joslin, J., et al. (2009). Use of stored carbon reserves in growth of temperate tree roots and leaf buds: Analyses using radiocarbon measurements and modeling. *Global Change Biology*, *15*(4), 992–1014. https://doi.org/10.1111/j.1365-2486.2008.01736.x

Gea-Izquierdo, G., Bergeron, Y., Huang, J.-G., Lapointe-Garant, M.-P., Grace, J., & Berninger, F. (2014). The relationship between productivity and tree-ring growth in boreal coniferous forests. *Boreal Environment Research*, *19*, 363–378.

Goudiaby, V., Schneider, R., Brais, S., Raulier, F., & Berninger, F. (2022). Understanding effects of competition and shade tolerance on carbon allocation with a carbon balance model. *Forests*, *13*(4), 572. https://doi.org/10.3390/f13040572

Guillemot, J., Francois, C., Hmimina, G., Dufrêne, E., Martin-StPaul, N. K., Soudani, K., et al. (2017). Environmental control of carbon allocation matters for modelling forest growth. *New Phytologist*, *214*(1), 180–193. https://doi.org/10.1111/nph.14320

Hartmann, H., & Trumbore, S. (2016). Understanding the roles of nonstructural carbohydrates in forest trees–from what we can measure to what we want to know. *New Phytologist*, *211*(2), 386–403. https://doi.org/10.1111/nph.13955

Hölttä, T., Mäkinen, H., Nöjd, P., Mäkelä, A., & Nikinmaa, E. (2010). A physiological model of softwood cambial growth. *Tree Physiology*, *30*(10), 1235–1252. https://doi.org/10.1093/treephys/tpq068

Huang, J. G., Ma, Q., Rossi, S., Biondi, F., Deslauriers, A., Fonti, P., et al. (2020). Photoperiod and temperature as dominant environmental drivers triggering secondary growth resumption in Northern Hemisphere conifers. *Proceedings of the National Academy of Sciences of the United States of America*, *117*(34), 20645–20652. https://doi.org/10.1073/pnas.2007058117

Huang, M., Piao, S., Ciais, P., Peñuelas, J., Wang, X., Keenan, T. F., et al. (2019). Air temperature optima of vegetation productivity across global biomes. *Nature Ecology & Evolution*, *3*(5), 772–779. https://doi.org/10.1038/s41559-019-0838-x

Ma, J., Shugart, H. H., Yan, X., Cao, C., Wu, S., & Fang, J. (2017). Evaluating carbon fluxes of global forest ecosystems by using an individual tree-based model FORCCHN. *Science of the Total Environment*, *586*, 939–951. https://doi.org/10.1016/j.scitotenv.2017.02.073

Merganičová, K., Merganič, J., Lehtonen, A., Vacchiano, G., Sever, M. Z. O., Augustynczik, A. L., et al. (2019). Forest carbon allocation modelling under climate change. *Tree Physiology*, *39*(12), 1937–1960. https://doi.org/10.1093/treephys/tpz105

Moffat, A. M., Papale, D., Reichstein, M., Hollinger, D. Y., Richardson, A. D., Barr, A. G., et al. (2007). Comprehensive comparison of gap-filling techniques for eddy covariance net carbon fluxes. *Agricultural and Forest Meteorology*, *147*(3–4), 209–232. https://doi.org/10.1016/j.agrformet.2007.08.011

Mund, M., Kutsch, W., Wirth, C., Kahl, T., Knohl, A., Skomarkova, M., & Schulze, E.-D. (2010). The influence of climate and fructification on the inter-annual variability of stem growth and net primary productivity in an old-growth, mixed beech forest. *Tree Physiology*, *30*(6), 689–704. https://doi.org/10.1093/treephys/tpq027

Munger, W., & Hadley, J. (2022). CO_2 profile at Harvard forest HEM and LPH towers since 2009. In *Harvard forest data archive: HF197* (Vol. *18*).

Munger, W., & Wofsy, S. (2020a). Biomass inventories at Harvard forest EMS tower since 1993. In *Harvard forest data archive: HF069*.

Munger, W., & Wofsy, S. (2020b). Canopy-atmosphere exchange of carbon, water and energy at Harvard forest EMS tower since 1991. In *Harvard forest data archive: HF004* (Vol. *32*).

Pastorello, G., Trotta, C., Canfora, E., Chu, H., Christianson, D., Cheah, Y. W., et al. (2020). The FLUXNET2015 dataset and the ONEFlux processing pipeline for eddy covariance data. *Scientific Data*, *7*, 1–27.

Poorter, L., & Kitajima, K. (2007). Carbohydrate storage and light requirements of tropical moist and dry forest tree species. *Ecology*, *88*(4), 1000–1011. https://doi.org/10.1890/06-0984

Portsmuth, A., & Niinemets, Ü. (2007). Structural and physiological plasticity in response to light and nutrients in five temperate deciduous woody species of contrasting shade tolerance. *Functional Ecology*, *21*(1), 61–77. https://doi.org/10.1111/j.1365-2435.2006.01208.x

Pothier, D. (2017). Relationships between patterns of stand growth dominance and tree competition mode for species of various shade tolerances. *Forest Ecology and Management*, *406*, 155–162. https://doi.org/10.1016/j.foreco.2017.09.066

Quéré, C. L., Andrew, R. M., Friedlingstein, P., Sitch, S., Pongratz, J., Manning, A. C., et al. (2018). Global carbon budget 2017. *Earth System Science Data*, *10*(1), 405–448. https://doi.org/10.5194/essd-10-405-2018

Raczka, B. M., Davis, K. J., Huntzinger, D., Neilson, R. P., Poulter, B., Richardson, A. D., et al. (2013). Evaluation of continental carbon cycle simulations with North American flux tower observations. *Ecological Monographs*, *83*(4), 531–556. https://doi.org/10.1890/12-0893.1

Reich, P. B., Tjoelker, M. G., Machado, J.-L., & Oleksyn, J. (2006). Universal scaling of respiratory metabolism, size and nitrogen in plants. *Nature*, *439*(7075), 457–461. https://doi.org/10.1038/nature04282

Richardson, A. D., Carbone, M. S., Keenan, T. F., Czimczik, C. I., Hollinger, D. Y., Murakami, P., et al. (2013). Seasonal dynamics and age of stemwood nonstructural carbohydrates in temperate forest trees. *New Phytologist*, *197*(3), 850–861. https://doi.org/10.1111/nph.12042

Rocha, A. V., Goulden, M. L., Dunn, A. L., & Wofsy, S. C. (2006). On linking interannual tree ring variability with observations of whole-forest CO_2 flux. *Global Change Biology*, *12*(8), 1378–1389. https://doi.org/10.1111/j.1365-2486.2006.01179.x

Schiestl-Aalto, P., Kulmala, L., Makinen, H., Nikinmaa, E., & Makela, A. (2015). CASSIA--a dynamic model for predicting intra-annual sink demand and interannual growth variation in Scots pine. *New Phytologist*, *206*(2), 647–659. https://doi.org/10.1111/nph.13275

Schiestl-Aalto, P., Ryhti, K., Mäkelä, A., Peltoniemi, M., Bäck, J., & Kulmala, L. (2019). Analysis of the NSC storage dynamics in tree organs reveals the allocation to belowground symbionts in the framework of whole tree carbon balance. *Frontiers in Forests and Global Change*, *2*, 17. https://doi.org/10.3389/ffgc.2019.00017

Teets, A., Fraver, S., Hollinger, D. Y., Weiskittel, A. R., Seymour, R. S., & Richardson, A. D. (2018). Linking annual tree growth with eddy-flux measures of net ecosystem productivity across twenty years of observation in a mixed conifer forest. *Agricultural and Forest Meteorology*, *249*, 479–487. https://doi.org/10.1016/j.agrformet.2017.08.007

Walters, M. B., & Reich, P. B. (1999). Research review. Low-light carbon balance and shade tolerance in the seedlings of woody plants: Do winter deciduous and broad-leaved evergreen species differ? *New Phytologist*, *143*(1), 143–154. https://doi.org/10.1046/j.1469-8137.1999.00425.x

Wilkinson, M., Eaton, E., Broadmeadow, M., & Morison, J. (2012). Inter-annual variation of carbon uptake by a plantation oak woodland in south-eastern England. *Biogeosciences*, *9*(12), 5373–5389. https://doi.org/10.5194/bg-9-5373-2012

Wright, I. J., Reich, P. B., Westoby, M., Ackerly, D. D., Baruch, Z., Bongers, F., et al. (2004). The worldwide leaf economics spectrum. *Nature*, *428*(6985), 821–827. https://doi.org/10.1038/nature02403

Würth, M. K., Pelaez-Riedl, S., Wright, S. J., & Körner, C. (2005). Non-structural carbohydrate pools in a tropical forest. *Oecologia*, *143*(1), 11–24. https://doi.org/10.1007/s00442-004-1773-2

Xu, X., & Trugman, A. T. (2021). Trait-based modeling of terrestrial ecosystems: Advances and challenges under global change. *Current Climate Change Reports*, *7*, 1–13. https://doi.org/10.1007/s40641-020-00168-6

References From the Supporting Information

Kaduk, J., & Heimann, M. (1996). Assessing the climate sensitivity of the global terrestrial carbon cycle model SILVAN. *Physics and Chemistry of the Earth*, *21*(5–6), 529–535. https://doi.org/10.1016/s0079-1946(97)81153-6

Oikawa, T. (1985). Simulation of forest carbon dynamics based on a dry-matter production model. *The Botanical Magazine=Shokubutsu-Gaku-Zasshi*, *3*, 225–238. https://doi.org/10.1007/bf02488773

Ogawa, H. (1969). An attempt at classifying forest types based on the relationship between tree height and DBH. *Comparative Study of Primary Productivity in Forest Ecosystems*, *00*, 3–17.

Ruimy, A., Dedieu, G., & Saugier, B. (1996). TURC: A diagnostic model of continental gross primary productivity and net primary productivity. *Global Biogeochemical Cycles*, *10*(2), 269–285. https://doi.org/10.1029/96gb00349

Schiestl-Aalto, P., Nikinmaa, E., & Mäkelä, A. (2013). Duration of shoot elongation in Scots pine varies within the crown and between years. *Annals of Botany*, *112*(6), 1181–1191. https://doi.org/10.1093/aob/mct180

Sheikh, V., Visser, S., & Stroosnijder, L. (2009). A simple model to predict soil moisture: Bridging event and continuous hydrological (BEACH) modelling. *Environmental Modelling & Software*, *24*(4), 542–556. https://doi.org/10.1016/j.envsoft.2008.10.005

Wang, X., Fang, J., Tang, Z., & Zhu, B. (2006). Climatic control of primary forest structure and DBH–height allometry in Northeast China. *Forest Ecology and Management*, *234*(1–3), 264–274. https://doi.org/10.1016/j.foreco.2006.07.007